Searching for SUSY in all hadronic final states with the α_T variable

Bryn Mathias
Imperial College London

Supervisor: Dr Alex Tapper

Abstract

This is a thesis.

Declaration

There are many like it.

Author

Acknowledgements

Thanks.

Contents

Chapter 1

Introduction

The accelerator and detectors The Large Hadron Collider (LHC) [3] is a proton-proton collider which is situated in the Large Electron Positron (LEP) tunnel approximately 100 m under the franco-swiss border. Design center of mass energy is 14 TeV with an instantaneous luminosity of $1 \times 10e^{34} cm^{-2} s^{-1}$. However during 2011 the center of mass energy was 7 TeV and the maximum luminosity was $5 \times 10e^{33}$ $cm^{-2} s^{-1}$. To achieve this high energy and high beam current the LHC uses superconducting niobium-titanium magnets, cooled to a temperature of 1.8 Kelvin, that produce a maximum field strength of 8.36 Tesla.

TODO: we might well need some more stuff about the LHC its self in here!

Situated around the LHC ring are four detectors, two general detectors ATLAS [1] and CMS (see Chapter 3 for a detailed discussion of the CMS detector) [7][11] which are designed to measure the standard model to high precision and search for new physics. The LHC beauty experiment [9] is designed to study at previously unattainable precision the decays of heavy quark flavors, both to measure the standard model couplings and to search for beyond the standard model (BSM) physical processes. Finally the ALICE [2] experiment is designed to run when the LHC is running in it's secondary mode where rather than proton bunches, lead ions are collided, in an effort to study the quark-gluon plasma.

New physics Whilst the theory of the standard model and of new physics models will be discussed in chapter 2 it is prudent to discuss the observable features of these models with regard to design requirements for the general purpose detectors.

Chapter 2

Theory

Chapter 3

The CMS detector

3.1 The High Level Trigger System

Chapter 4

Offline Object Reconstruction and Identification.

4.1 Hadronic Jets.

AK5 calo jets – explanation of the jet algos. How they are clustered at CMS. No need to mention PF? (we don't use it so why bother). Energy resolution, Jet energy corrections, ID. 2011 note

4.2 Electrons.

GSF elections - ID, use tracking. Veto on elections. 2011 note

4.3 Muons.

GPT muons - exact ID's, reconstruction methods. both veto and used to collect the control sample. 2011 note

4.4 Photons.

Veto and control sample - noise and spike cleaning 2011 note

4.5 Noise cleaning.

Dead ecal sections. monsters. Trackless events. 2011 note.

Chapter 5

Level One Calorimeter Trigger

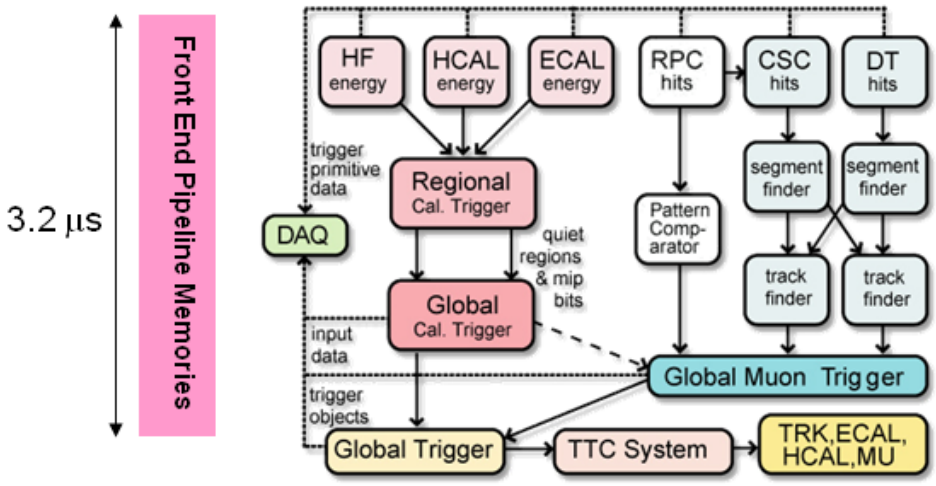

Figure 5.1: The CMS Level-1 Trigger system

The CMS Level-1 trigger system[4] is a pipelined dead-timeless system based on custom-built electronics. The Level-1 trigger is a combination of several sub systems, which are interconnected as depicted in Figure 5.1.

Corse grain information from the electro-magnetic, hadronic and forward calorimeters is processed by the Regional Calorimeter Trigger (RCT), this is then passed to the Global Calorimeter Trigger (GCT) where the corse grain information is clustered in to physics objects, these objects are then passed to the Global Trigger where the Level-1 accept decision is made. Due to the limited size of the pipe line this Level-1 accept must be issued within 4.0 μs.

The objects passed from the GCT to the GT include electro-magnetic objects, both electrons and photons as due to the lack of tracking information at the Level-1 trigger these objects are indistinguishable, jets and energy sums.

The RCT generates up to 72 isolated and non-isolated electro-magnetic objects, these are sorted by rank, which is equivalent to transverse energy E_{T}. The four highest ranked electro-magnetic objects are then passed via the GCT to the GT at an equivalent data rate of 29 Gbs^{-1} per type.

Hadronic objects under go two clustering steps. First the transverse energy sums of the ECAL and corresponding HCAL towers are calculated, the towers are then summed in to 4×4 trigger regions, these are passed to the GCT at a data rate of 172.8 Gbs^{-1}. These trigger regions are clustered in to jet candidates by the GCT and ranked. The jets are then sub-divided in the categories depending on their pseudo-rapidity and the result of τ identification.

Energy sums come in two forms, the total transverse energy E_{T} which is the scalar sum of all transverse energies and the total jet transverse energy H_{T} which is calculated as the scalar sum of all jets above some programable threshold.

The missing energy equivalents of these $\not{E}_{\mathrm{T}}$ and $\not{H}_{\mathrm{T}}$ are formed from the negative vector sum of the objects considered for the transverse sums.

5.1 Leve-1 Trigger Jet Algorithm

FIXME: This is taken pretty much straight from [8] might want to steal less??

The CMS detector can be un-rolled in the ϕ direction to form a rectangular grid of the 396 calorimeter regions, connected along the ϕ edge. The rectangle is formed from 18 ϕ divisions (from $-180° < \phi \leq 180°$) and 22 η divisions (from $-5 < \eta < 5$). Each ϕ division corresponds to 20°. The η divisions correspond to $\Delta\eta = 0.5$ in the forward calorimeters and to $\Delta\eta \approx 0.348$ in the barrel. A pictorial representation of this can be seen in figure 5.3.

A jet candidate is created if the sum of the ECAL and HCAL energies of the central calorimeter region has an energy deposit larger than all of its neighbours, as shown in figure 5.2 The jet is centered at this region where $p_T^{central} > p_T^{surrounding}$ and the transverse

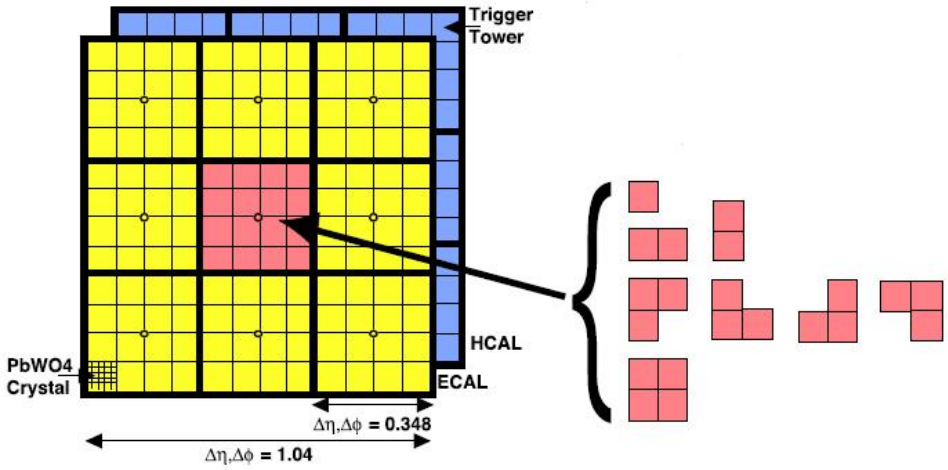

Figure 5.2: The 3 × 3 jet-finder window at Level-1. Each cell represents a trigger tower, which is the sum of the HCAL and ECAL transverse energies. The τ-jet veto patterns are shown to the right.

energies of the surrounding regions are summed in to the central region. The jet is then classified as a τ jet if $|\eta| < 3.0$ and none of the τ veto bits are set. If any τ vetoes are set the jet is classified as a central jet. The jet is classified as forward if $3.0 < |\eta| < 5.0$

The τ-vetoes are set by the RCT depending on whether or not the energy depositions in up to four contiguous trigger towers are below a programmable fraction of the regional E_{T} as shown in Figure 5.2.

It is possible to apply separate jet energy corrections to each of the sub categories of GCT jets, however at current the same E_{T} and η dependant corrections are used for all three jet types. These corrections are discussed in detail in Section **??**

In order to reduce the total data duplicated and shared between the jet finders the GCT employs a pre-clustering algorithm, which involves 18 jet finders operating simultaneously over the whole detector. These jet finders then only share information with neighbouring regions when the clustered jets are found. Figure 5.3 shows the boundaries between which the jet finders operate, these map naturally on to one RCT crate per jet finder. A maximum of 3 jets can be found on each of the ϕ strips acted on by the jet finders, this gives a maximum of 108 jets per event. In order to preserve continuity across the $\eta = 0$ boundary, the two adjacent trigger regions are shared between the jet finders.

An example of the jet finding is shown in Figure 5.4. The first step is to create a 2×3 mini cluster around any local maxima found in the 12×2 strip. Equality statements are

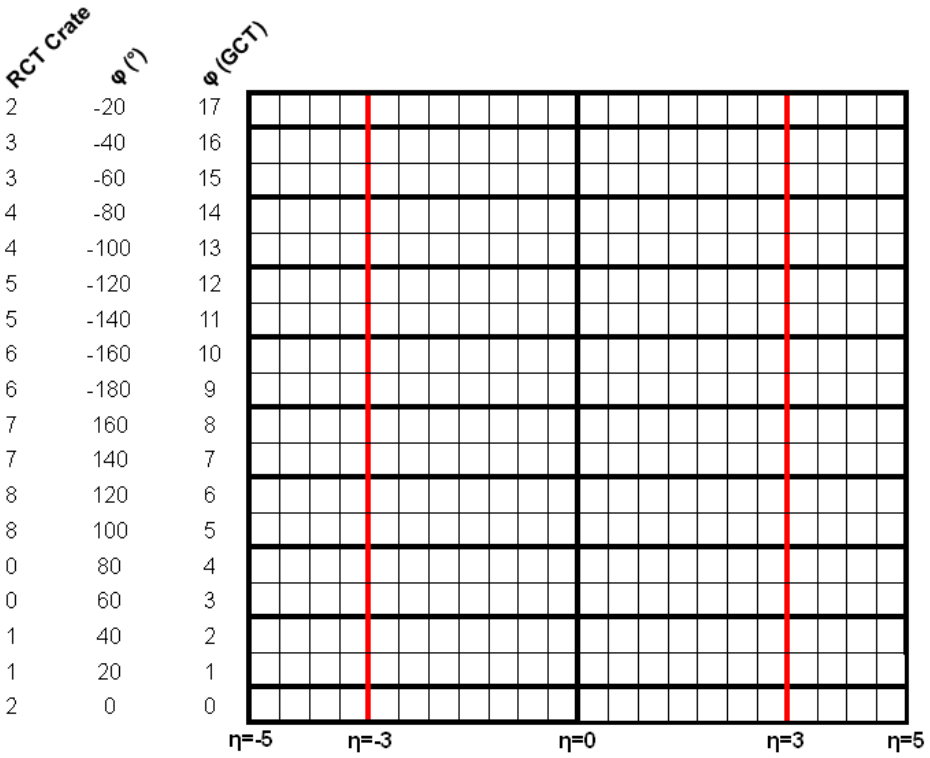

Figure 5.3: The calorimeter map that the 3 × 3 jet-finder operates over is made up for 396 calorimeter regions, each jet finder is mapped on to an RCT crate which is composed of an 11 × 2 strip of these regions. RCT crate labels are shown for negative η only.

imposed so that the central cell is greater than its neighbours in some directions and greater than or equal to the neighbours other directions to enforce a gap of at least one trigger region in both η and ϕ between the centres of the clustered jets.

In the second step the jet finder transfers the three largest mini clusters on a given ϕ strip to the closest ϕ strip on the neighbouring jet finder. These are then compared against the existing mini clusters in that ϕ strip, those that are adjacent or diagonally adjacent to a larger mini cluster are removed. The inequalities statements are then reimposed to prevent problems with clusters having the same energies. In the final stages the mini clusters have their three adjacent regions summed in to produce a 3 × 3 jet cluster. Finally the four highest ranked jets are corrected and passed to the GT.

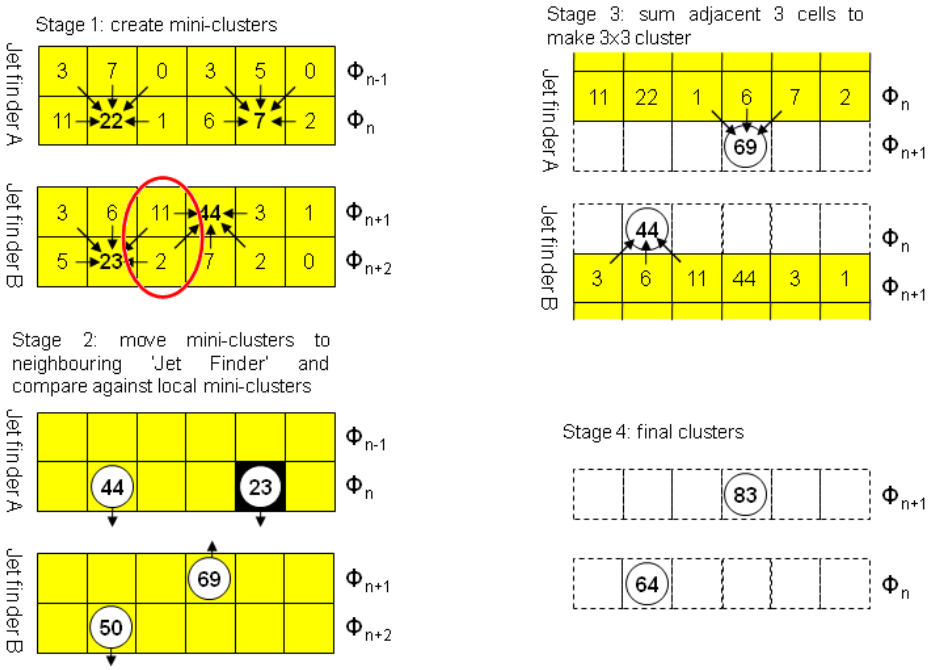

Figure 5.4: The Level-1 jet clustering method, six cells in η are shown. An example of overlapping jets is shown

5.2 Level-1 Trigger Performance

During the start of data taking in 2010, no Jet Energy Corrections (JEC's) were applied in the Level-1 trigger. This gave a relatively slow turn on in therms of offline hadronic objects. During the winter shut down of the LHC between the 2010 and 2011 running periods a set of Level-1 JEC's were developed. These corrections used a peicewise cubic form for the interpolation function used to correct the jet energy dependant on it's uncorrected E_{T} and η values. However as can be seen in Figure 5.5 these corrections were only applied to jets with a raw energy below 130 GeV.

To overcome this a new set of corrections were derived using a well established tool for producing offline corrections, **REFERENCE TO tapper-001 here** using the same functional form that was derived for correcting particle flow jets. **REFERENCE TO PF HERE** In this section we discuss the performance of both sets of Level-1 JEC's and the performance of the energy sum trigger H_{T}, $\not{H}_{\mathrm{T}}$, and $\not{E}_{\mathrm{T}}$, the performance of which are not effected by the application of jet energy corrections at the Level-1 trigger due to the quantities being built from the internal GCT jets before they pass though the corrections look up table. The performance is studied under both low pile up conditions

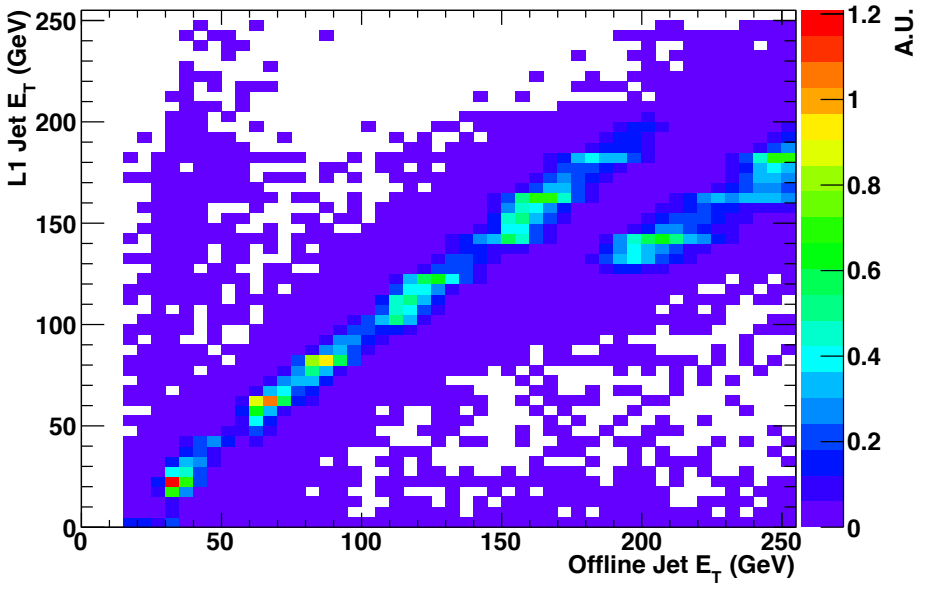

Figure 5.5: Correlation between offline corrected jet energy and Level-1 corrected jet energy for matched jets. The discontinuity shows where the Level-1 jet corrections do not alter the raw energy of the jet.

where the mean peak pile up $< PU >$ is 16 primary vertices and under high pile up conditions where $< PU >$ is 36 primary vertices.

To measure the performance of the Level-1 single jet triggers we assume that the leading offline corrected anti-k$_t$(0.5) calorimeter jet is the jet that triggered the event. We then match this offline jet to the closest Level-1 jet in ΔR, where for there to be a match $\Delta R < 0.5$ is required. For this match central, τ and forward jets are considered. Events where the recorded Level-1 energy is set to the overflow bit, meaning they have more than 254 GeV of E_{T} measured at Level-1 are ignored.

To collected an unbiased sample in which to measure the performance, two methods are used; the first is to require a Minimum Bias trigger, which is triggered by beam induced activity in the CMS detector. However due to the nature of these events the number of interactions with high energy interactions is low and the prescale applied to this trigger further reduces the sample size. However this method does produce the least bias. The second method is to trigger an object that does not deposit signifiant energy in the calorimeter systems, in this case we choose the trigger with the lowest un prescaled p_{T} threshold. The muon trigger is chosen with some loose isolation requirements to make sure it does not overlap with a jet, causing a discrepancy in the measure of the

calorimetric energy. The sample has a higher number of events due to the large amount of bandwidth given to the single object muon triggers in CMS. The use of a muon trigger also serves to increase the precision of the measurement of the Level-1 missing energy trigger as the muons are not seen by the calorimeter system the $\not{E}_{\mathrm{T}}$ sample is enriched.

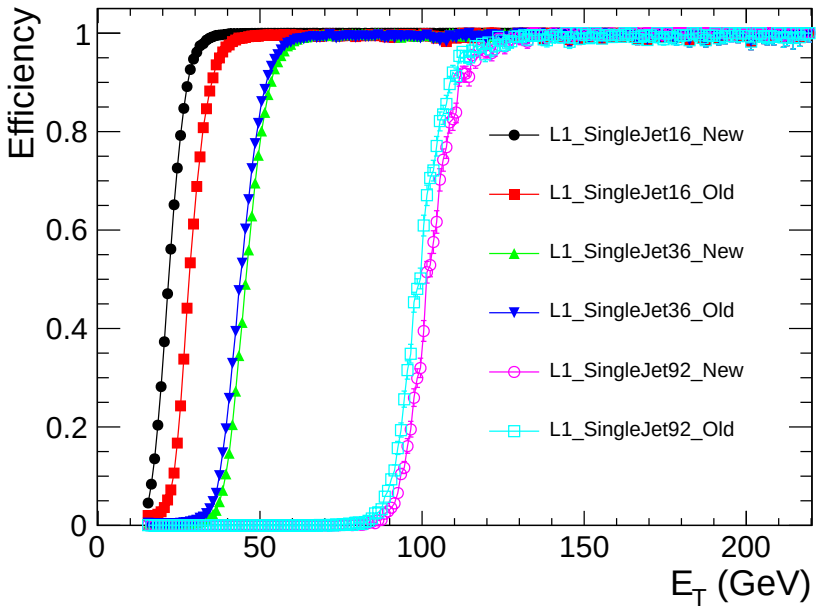

Figure 5.6: Comparison of the performance of L1_SingleJet16, L1_SingleJet36 and L1_SingleJet92, when using the piecewise cubic corrections and using the new correction scheme. The performance of the two is negligible above 36 GeV.

Figure 5.6 shows the performance of the piecewise cubic corrections (PWC) and the performance of the new corrections. The data was taken with the PWC enabled in the GCT hardware. The updated corrections were emulated in the bitwise reproduction of the GCT. The made an event by event comparison possible. At low E_{T} the new corrections turn on before the PWC corrections, if the new corrections were applied on with no change to the trigger menu, the Level-1 trigger rate would rise. At a threshold of 36 GeV and higher the performance of the two correction schemes is very similar. Due to the small change in observed performance and the ability to correct raw energies above 130 GeV, the new corrections were deployed online at the start of Run2011B and are still online at the end of data taking in 2012.

The performance of the updated corrections was then measured with data taken with the corrections applied in the GCT hardware. The reference sample was taken with the `HLT_IsoMu24_v*` high level muon trigger. The performance of three example triggers is show in Figure 5.7, these curves are fitted with an error function, which is not a perfect

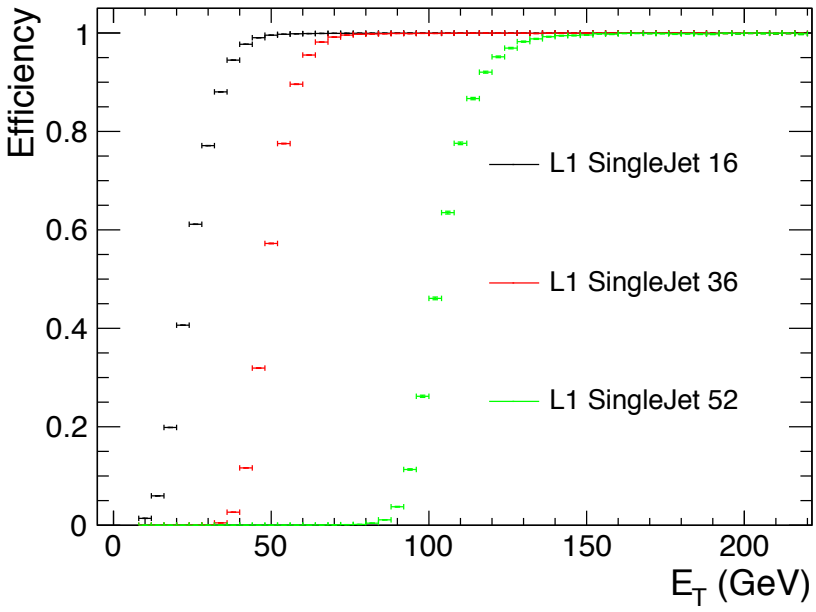

Figure 5.7: Performance measurements of L1_SingleJet16, L1_SingleJet36 and L1_SingleJet92, when using the new correction scheme deployed in the GCT hardware. The performance is slightly worse than that of the emulated triggers due to a change in pile up conditions between the two data taking periods.

description of the turn on, but does give some guiding figures as to the performance of the triggers. The data collected and represented in Figure 5.7 has a peak mean pile up ($< PU >$) of 16 interactions, this is higher than the $< PU >$ of approximately 8-10 which were the running conditions in Run2011A, on which the previous comparison was performed. The observed difference in the performance of the Level-1 single jet triggers as a function of pile up is a case of concern when data taking is underway at the LHC's design luminosity, where $< PU >$ is >36 at an instantaneous luminosity of $1{\times}10^{34} cm^{-27} s^{-1}$.

The instantaneous luminosity in 2012 was predicted to be $5{\times}10^{33} cm^{-27} s^{-1}$, with $< PU > \approx 32$. In order to study the effect on the trigger rate and efficiency a high pile up, low instantaneous luminosity, LHC fill was taken in 2011.

The Level-1 single jet performance was studied in this run in terms of two offline object definitions. The first was the standard anti-k$_t$(0.5) calorimeter jet reconstruction, the second was a set of anti-k$_t$(0.5) calorimeter jets which were corrected for pile up using the fastjet correction algorithm, **cite fast jet** which is further detailed in Section 4. The fast-jet corrections remove the energy deposited in the secondary interactions from the objects which are expected to come from the primary hard interaction, thus removing

energy from the offline jets. The effect of these pile up corrections on the Level-1 trigger performance is first studied under conditions with $< PU >$ of 16, the performance of which has already been measured with respect to non pile up corrected offline objects, as a sanity check. The results are shown in Figure 5.8 , the performance is measured with respect to `HLT_IsoMu24_v*`, in terms of both pile up corrected and standard offline objects. As expected the performance in the two cases is very similar. The same comparison is shown for H_{T} in Figure 5.9, where the effect of the fastjet corrections is more pronounced due to the sum over jets. The difference between the turn on points for the two offline quantities is on the order of 10 GeV under low pile up conditions.

Due to the high pile up fill being a specialised fill with low instantaneous luminosity, the high level trigger paths were disabled, instead Level-1 trigger pass though paths were utilised to take the data. The Level-1 single muon pass though trigger is used to collect the reference sample. Otherwise the same analysis method is common between the two data sets. Figure 5.10 shows the difference in turn on for three example Level-1 single jet triggers when using standard calorimeter jets and fastjet corrected calorimeter jets. In the high pile up conditions the switch to offline jets that are corrected for pile up shifts the turn on point to lower vales of E_{T}, the magnitude of this effect reduces as the Level-1 trigger trigger threshold raises. This implies that the same offline performance as seen in the low pile up conditions can be achieved by using the pile up corrected offline objects and raising the Level-1 single jet trigger thresholds.

Figure 5.11 shows the same high pile up comparison, but for the Level-1 H_{T} triggers. Due to the size of the sample the precision of this measurement is low. However the same trend of a shift to lower H_{T} values of the turn on point of the Level-1 triggers when using pile up corrected offline objects is observed. This again implies that the Level-1 H_{T} trigger thresholds can be raised whilst preserving the same offline performance as during the low pile up conditions.

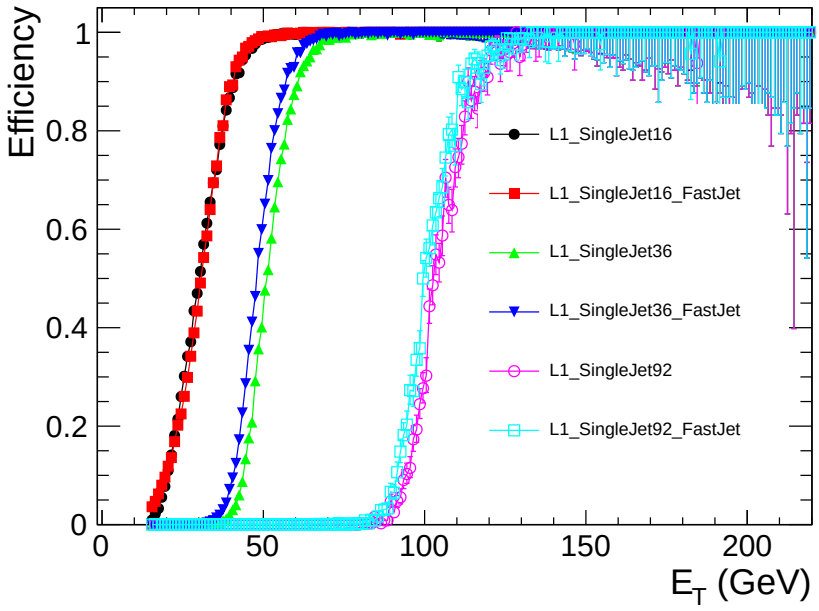

Figure 5.8: Comparison of the performance of L1_SingleJet16, L1_SingleJet36 and L1_SingleJet92 triggers. Where $< PU > = 16$. For two offline reconstruction methods, standard anti-k$_t$(0.5) calorimeter jets and pile up corrected anti-k$_t$(0.5) calorimeter jets.

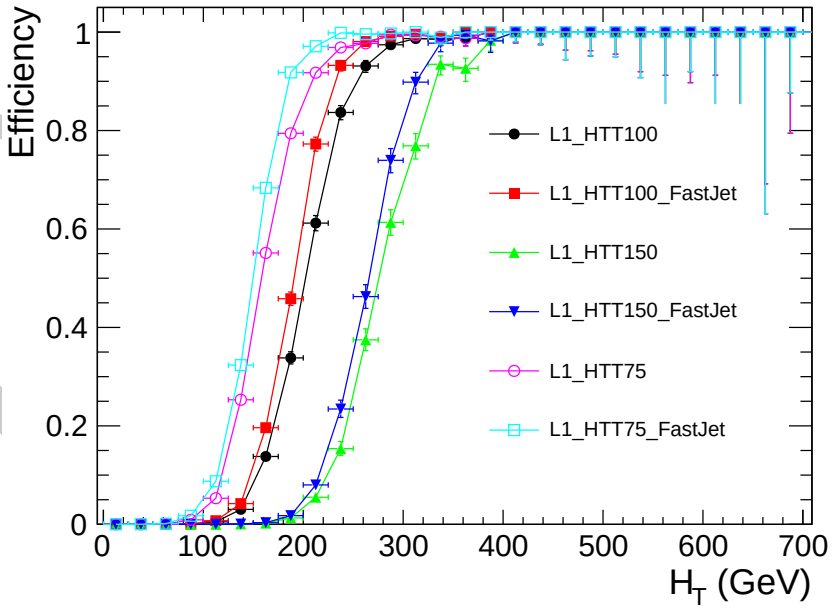

Figure 5.9: Comparison of the performance of L1_HTT75, L1_HTT100 and L1_HTT150 triggers. Where $< PU > = 16$. For two offline reconstruction methods, standard anti-k$_t$(0.5) calorimeter jets and pile up corrected anti-k$_t$(0.5) calorimeter jets.

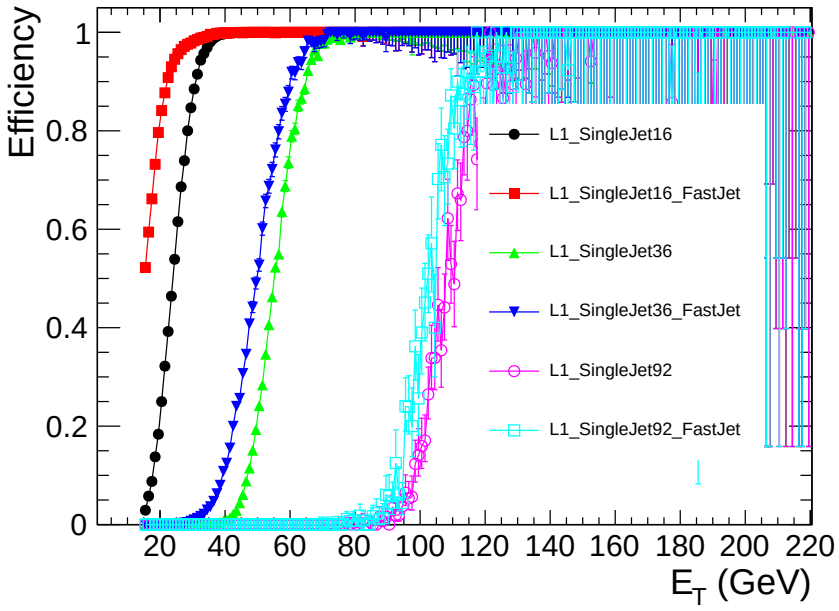

Figure 5.10: Comparison of the performance of L1_SingleJet16, L1_SingleJet36 and L1_SingleJet92 triggers. Where $< PU > = 36$. For two offline reconstruction methods, standard anti-k$_t$(0.5) calorimeter jets and pile up corrected anti-k$_t$(0.5) calorimeter jets.

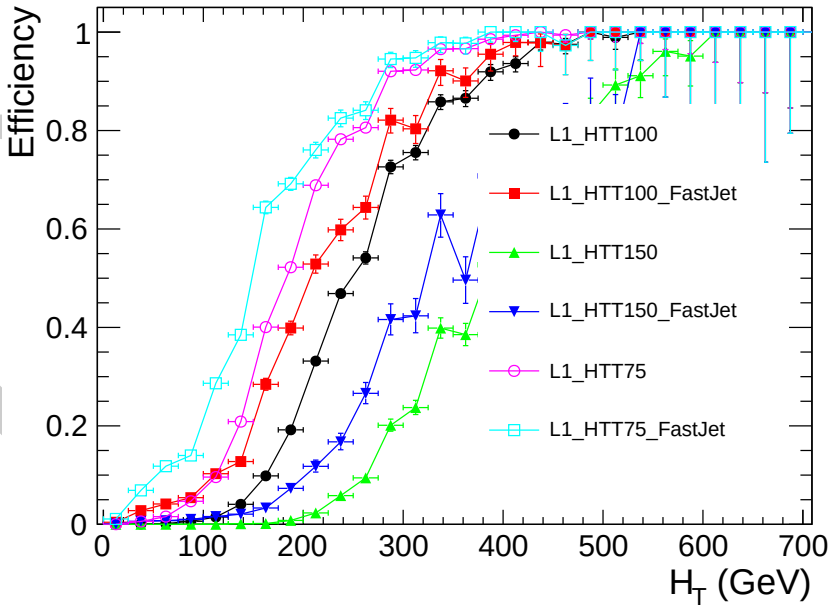

Figure 5.11: Comparison of the performance of L1_HTT75, L1_HTT100 and L1_HTT150 triggers. Where $< PU > = 36$. For two offline reconstruction methods, standard anti-k$_t$(0.5) calorimeter jets and pile up corrected anti-k$_t$(0.5) calorimeter jets.

5.3 Level-1 Trigger Pile-up Mitigation

Due to the lack of a requirement of a jet seed threshold, soft non-collimated jets, such as those expected in a high pile up environment are found. Trigger decisions are then made using these pile up jets.

This is less of a problem for the single jet triggers which have a high P_T threshold. However the H_{T} triggers, where $H_{\mathrm{T}} = \sum_{jets} E_T^{jet}$ and the requirement of $E_{\mathrm{T}}{}^{jet} \geq 10$ GeV is made, see a large increase in rate due to pile-up, this is due to the low energy threshold required for a jet to be added to the H_{T} sum.

To counteract the effect of pile up on trigger rate we study the effects of requiring a jet seed threshold on the rate and efficiency of the individual jet and H_{T} triggers.

Figure 5.2 depicts 3×3 trigger regions, each of which are built from 4×4 trigger towers. In this case the central region is the jet seed. The proposed change would require there to be a threshold energy in the seed region.

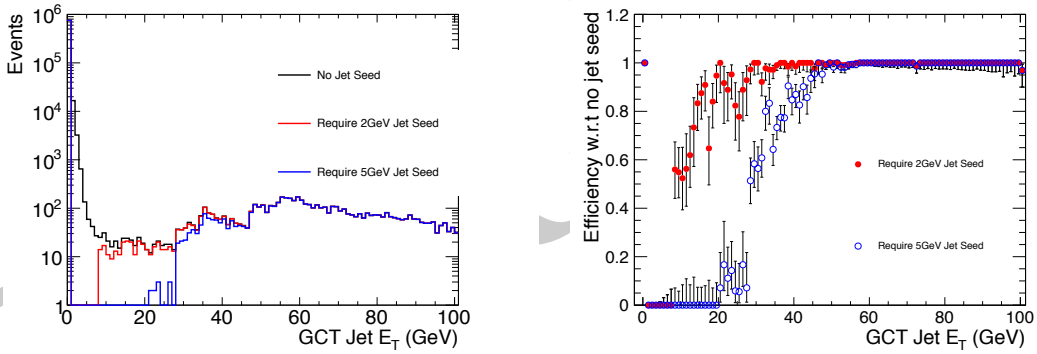

(a) GCT internal uncorrected jet E_{T} distributions for the same events with a 0, 2 or 5 GeV seed requirement.

(b) Efficiency of applying a requirement of 2 or 5 GeV with respect to no requirement.

Figure 5.12: Effect of requiring a jet seed threshold on GCT internal jets.

The study of using jet seed thresholds of 2 and 5 GeV is presented. Figure 5.12 shows how the different threshold requirements effect the rank of the internal GCT jets. The effect is to remove all jets below 2(5) GeV and to cut out jets from the low end of the distribution. From Figure 5.12(b) it is possible to see the point beyond which the requirement of a jet seed has no effect. For a cut of 2 GeV jets above an uncorrected E_{T} of ≈ 35 GeV are not effected, for a seed threshold of 5 GeV jets above an uncorrected E_{T} 55 GeV are not effected.

Table 5.1: Summary of rate reduction during low pile up conditions.

Trigger	% of rate taken with 2 GeV requirement	% of rate taken with 5 GeV requirement
L1_HTT100	$98.6 \pm 11.6\%$	$97.9 \pm 11.6\%$
L1_QuadJet38	$100.0 \pm 0.0\%$	$85.3 + 6.2 - 8.7\%$
L1_Jet50	$100.0 + 0.0 - 12.3\%$	$85.7 + 9.1 - 15.8\%$

5.3.1 Effect on trigger rates

The effects of applying a seed threshold are quantified in terms of the level of rate reduction in the Level-1 hadronic triggers. Three triggers are studied, they are:

- L1_SingleJet50 - Level one trigger requiring at least one jet with a corrected $E_{\mathrm{T}} \geq 50$ GeV.
- L1_HTT100 - Level one trigger requiring $H_{\mathrm{T}} \geq 100$ GeV.
- L1_QuadJet38 - Level one trigger requiring at least four jets in the event with $E_{\mathrm{T}} \geq 38$ GeV.

5.3.2 Low Pile Up

A small effect on trigger rates in the low pile up scenario is expected due to the majority of energy deposited in the calorimeters coming from hard scattering.

Table 5.1 shows the rate reduction of requiring a 2 or 5 GeV seed threshold with respect to requiring no seed threshold.

5.3.3 High Pile Up

Pile up is expected to add a small quantity of energy to the entire calorimeter system, this energy comes in the form of soft non-collimated jets. These objects are then not reconstructed if the topological cut of applying a seed threshold is required.

Table 5.2 shows the rate reduction of requiring a 2 or 5 GeV seed threshold with respect to requiring no seed threshold in high pile up conditions.

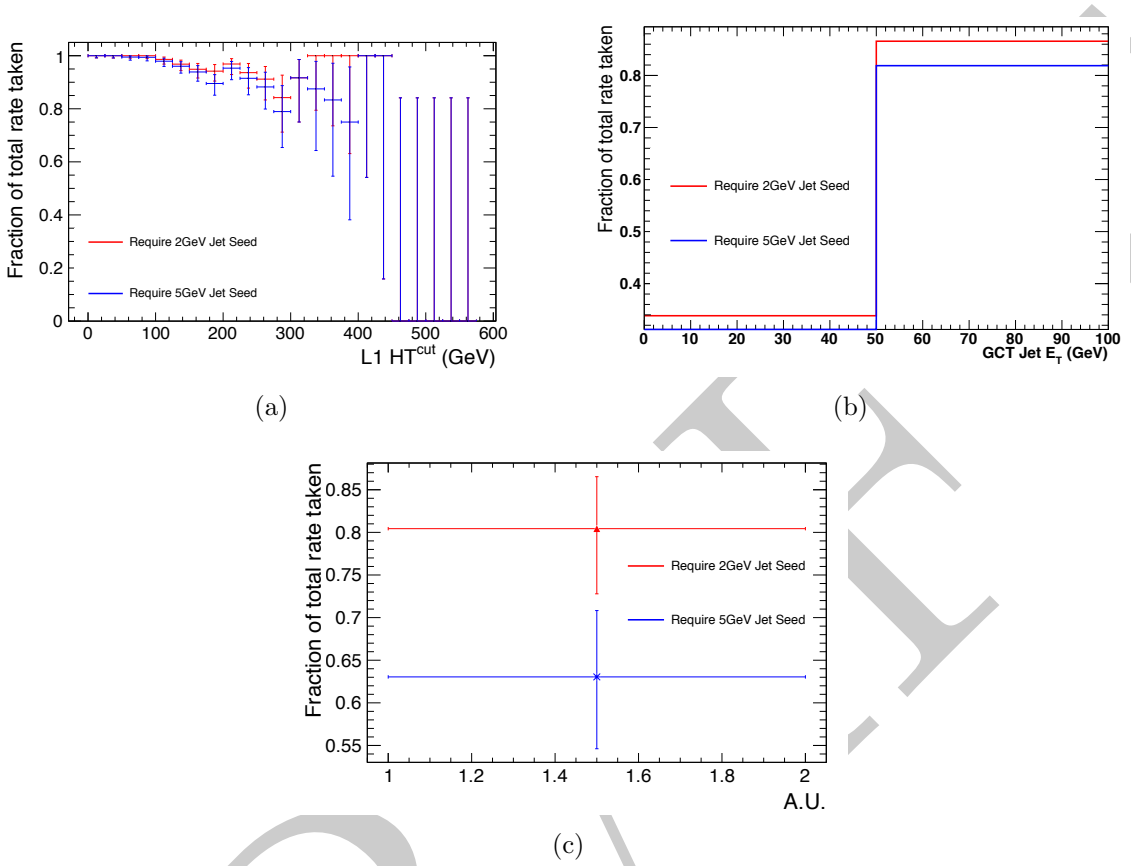

Figure 5.13: Rate reductions for various Level-1 algorithms when applying a 2,5 GeV seed tower requirement, in low pile up conditions. Figure (a) shows the rate reduction for H_{T} triggers at low pile up in cut steps of 25 GeV. Figure (b) shows the rate reduction for jets with in $|\eta| < 3.$ and $p_{\mathrm{T}} > 50$ GeV. Figure (c) shows the rate reduction for a quad jet trigger, with jet $|\eta| < 3.$ and $p_{\mathrm{T}} > 38$ GeV.

Table 5.2: Summary of rate reduction during high pile up conditions.

Trigger	% of rate taken with 2 GeV requirement	% of rate taken with 5 GeV requirement
L1_HTT100	$60.4 \pm 5.7\%$	$0.67 + / - 0.67\%$
L1_QuadJet38	$71.4 + 18.2 - 25.9\%$	$57.1 + 22.3 - 24.8\%$
L1_Jet50	$100.0 + 0.0 - 7.7\%$	$73.9 + 9.8 - 12.3\%$

5.3.4 Effect on trigger efficiency

Section 5.3.1 shows that requiring a jet seed threshold substantially reduces the trigger acceptance rate at in high pile up conditions.

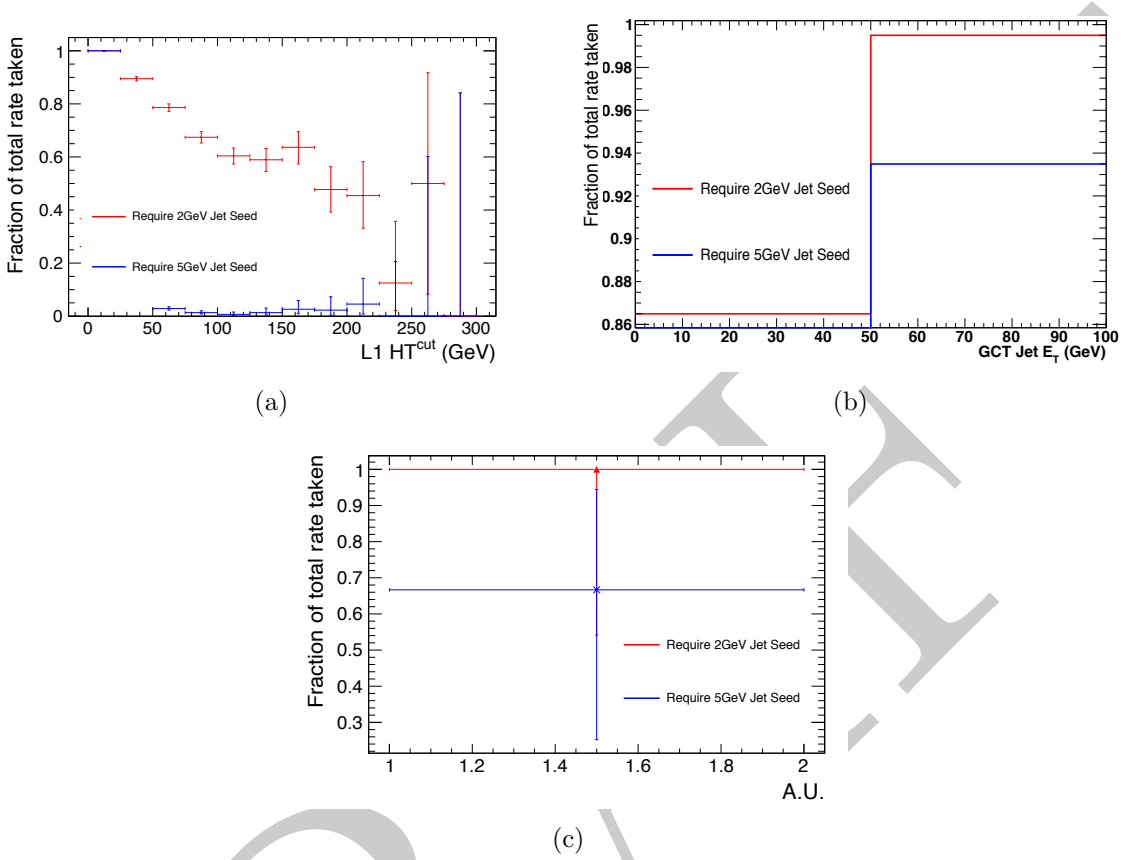

Figure 5.14: Rate reductions for various Level-1 algorithms when applying a 2,5 GeV seed tower requirement, in high pile up conditions. Figure (a) shows the rate reduction for H_{T} triggers at high pile up, in cut steps of 25 GeV. Figure (b) shows the rate reduction for jets with in $|\eta| < 3.$ and $p_{\mathrm{T}} > 50\,\mathrm{GeV}$. Figure (c) shows the rate reduction for a quad jet trigger, with jet $|\eta| < 3.$ and $p_{\mathrm{T}} > 38\,\mathrm{GeV}$

However the aim of requiring a jet seed is to reduce rate, but not at the cost of physics. In this section we look at the effects of requiring a seed threshold, whilst requiring some loose, generic offline selection on the hadronic objects.

The change in efficiency is measured under low pile up conditions where the least extra energy added to the event. This gives a worse case estimate of the effect of requiring a jet seed on the offline efficiency.

Each offline reconstructed calorimeter jet must adhere to the following quality criteria:

- Pass loose calorimeter ID
- $p_{\mathrm{T}} \geq 30$ GeV.
- $|\eta| \leq 3.0$.

- Matched to a Level-1 jet with $\Delta R \leq 0.5$.

Where loose calorimeter ID is defined as; Electro-Magnetic fraction > 0.01, fraction of energy in the Hybrid Photo Diodes < 0.98 and the number of n90hits > 1.

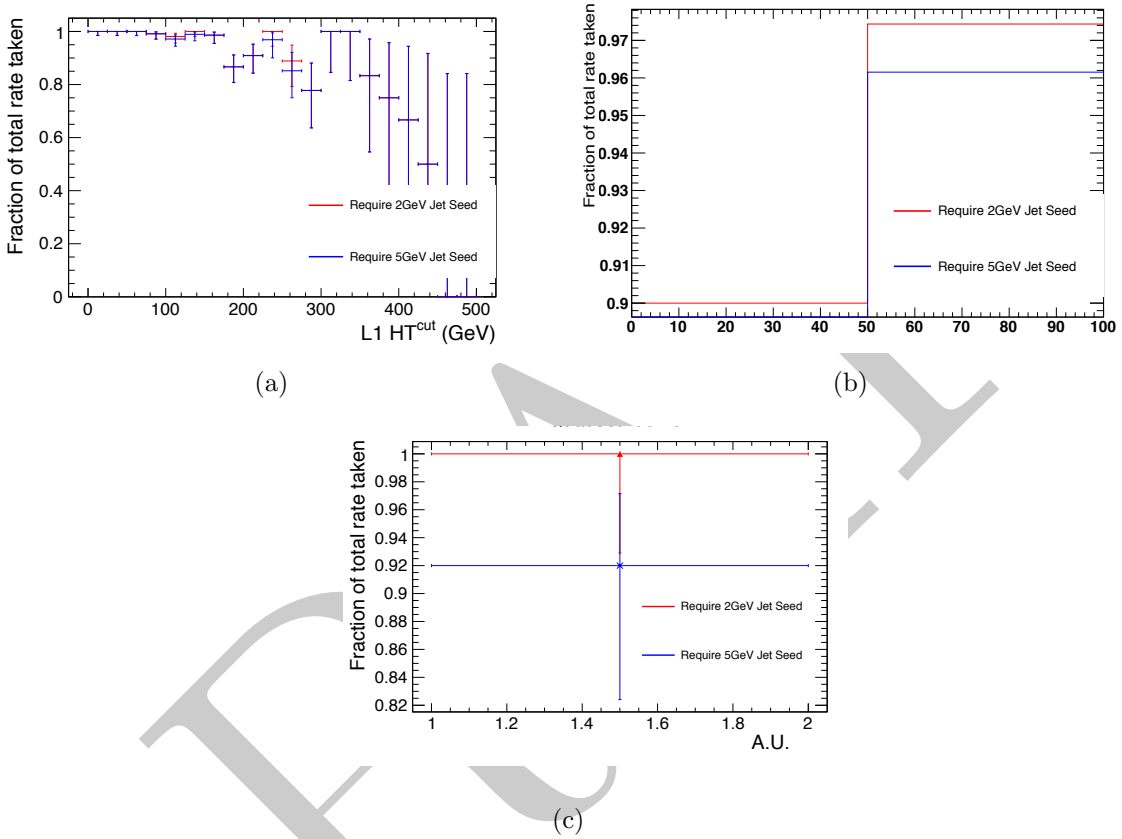

Figure 5.15: Efficiency reductions for various Level-1 algorithms when applying a 2 or 5 GeV seed tower requirement, in low pile up conditions. Figure (a) shows the efficiency reduction for H_{T} triggers at low pile up in cut steps of 25 GeV. Figure (b) shows the efficiency reduction for jets with in $|\eta| < 3.$ and $p_{\mathrm{T}} > 50\,\mathrm{GeV}$. Figure (c) show the efficiency reduction for a quad jet trigger, with jet $|\eta| < 3.$ and $p_{\mathrm{T}} > 38\,\mathrm{GeV}$.

Efficiency of H_{T} Triggers Figure 5.15(a) shows the acceptance reduction after applying the two jet seed thresholds. The distribution is the cumulative number of events passing a cut of $L1HT^{cut}$ in bins of 25 GeV. Due to H_{T} being the scalar sum of the jet p_{T}'s in the event the value of Level-1 H_{T} is reduced as jets are removed from the calculation. To preserve efficiency the Level-1 trigger threshold will have to be reduced. Comparing figures 5.13(a) and 5.15(a), if the trigger threshold is reduced to 75 GeV an efficiency of $\geq 95\%$ can be maintained whilst reducing the trigger rate by $\approx 2\%$ when

requiring a 2 GeV seed threshold and reduced by $\approx 3\%$ when requiring a 5 GeV seed threshold. When comparing to the high pile up rate reduction in figure 5.14(a) it is shown that the trigger rate can be reduced by $\approx 20\%$ when requiring a 2 GeV seed threshold and reduced by $\geq 99\%$ when requiring a 5 GeV seed threshold.

Efficiency of Jet Triggers Figure 5.15(b) shows the change in acceptance of jets in low pile up conditions when the two seed thresholds are required. The effect is on the order of a few percent for each of the thresholds. Requiring a 2 GeV seed reduces the efficiency for jets above 50 GeV by $\approx 2.5\%$, whilst requiring a 5 GeV seed reduces the efficiency of the same jets by $\approx 4\%$.

Efficiency of MultiJet Triggers Figure 5.15(c) shows that the effect of requiring a seed threshold of 2 GeV has no effect on the efficiency of the quad jet 38 GeV trigger and requiring a seed threshold of 5 GeV reduces the efficiency of the quad jet 38 trigger by 8%. The change in rate is dramatic in high pile up conditions where for a 2 GeV seed threshold the rate is reduced by $\approx 30\%$ and by $\approx 40\%$ when requiring a 5 GeV seed. However it is to be noted that the sample where this measurement has been made is of limited size, inferring a reasonably large statistical uncertainty.

5.3.5 Summary

The effects of requiring a jet seed have been studied using the Level-1 trigger emulator on high and low pile-up samples. The studies show that requiring a jet seed of 5 GeV greatly reduces the rate of the H_{T} and Multi Jet triggers in high pile up conditions, whilst not adversely effecting the data taking efficiency of these triggers.

The cross section of L1_HTT150 has been measured with and with out the addition of a jet seed threshold of 5 GeV as shown in Figure 5.16. Ideally the trigger cross section would be independent of the instantaneous luminosity and pile up, Figure 5.16 shows that the addition of a 5 GeV seed threshold reduces the dependance on instantaneous luminosity of the trigger cross section.

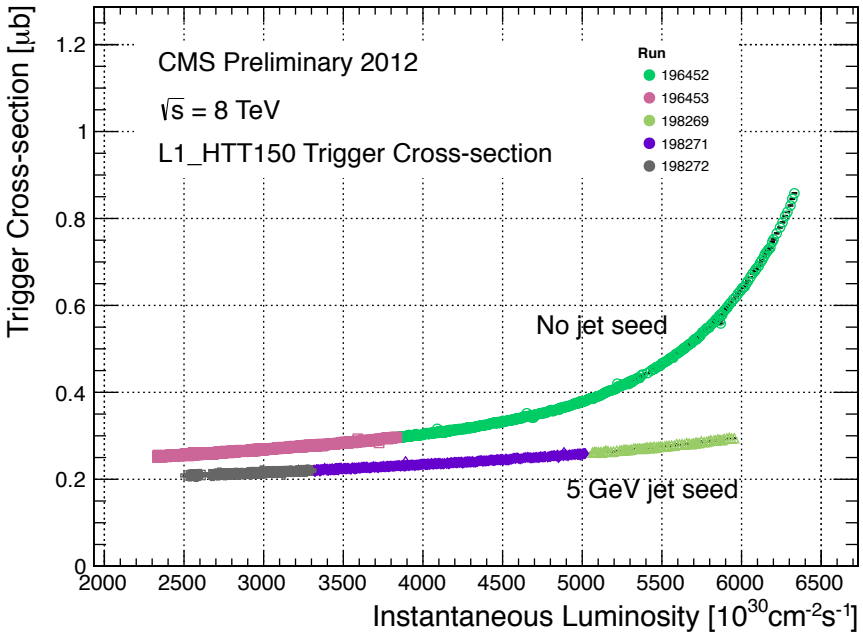

Figure 5.16: Trigger cross section as a function of number of pile up interactions. Showing that applying a 5 GeV jet seed threshold dramatically reduces the quadratic dependance of cross section on the number of pile up interactions

Chapter 6

High level triggers for the α_T analysis.

Chapter 7

The α_T analysis

In this chapter we discuss the main analysis performed as the subject of this thesis. For the theoretical motivations of this search please see Chapter 2. The analysis is based on the full 2011 data set which is made up of $5\,\text{fb}^{-1}$ of 7 TeV data. However $5\,\text{fb}^{-1}$ of the 2012 8 TeV is looked at to measure the performance of the upgraded α_T HLT paths.

7.1 The Problem

If Supersymmetry or some other beyond the standard model theory is to provide a yet undiscovered dark matter candidate, it is predicted that this candidate will interact via the weak nuclear force only. This gives a decay topology involving missing energy in the form of the dark matter particle escaping the detector. Due to the nature of interactions at the L.H.C, these particles would be produced at the end of a decay chain of heavy particles that interact strongly, giving a final topology involving hadronic objects which are classified as jets for the purpose of analysis and missing energy. There are several standard model processes that mimic this final state.

By far the largest of these backgrounds comes from QCD multi jet events where fake missing energy is introduced either from failures in reconstruction, or stochastic fluctuations in the calorimeter systems. **FIXME: expand on this - E /sqrt E has non gaussian tails. Figures of jets falling below threshold, missed jets etc. probably from some jet-met paper.** However due to the theoretical errors on the QCD production cross section predicting the number QCD background events from Montecarlo simulation is not possible. A secondary QCD background also exists, where due to the requirement of a jet E_{T} threshold, multiple jets fall under threshold by a few

GeV, this causes a balanced event to look unbalanced as the jets under threshold are no longer considered. The solution is then to devise a kinematic cut that removes these events from the signal selection.

The second major background comes from standard model electro-weak decays and is irreducible. The electro-weak decays that form the back ground are W $\rightarrow \tau\nu$ + Jets, where the τ is reconstructed as a jet, or the lepton fails the identification required for the dedicated lepton vetoes, Z $\rightarrow \nu\overline{\nu}$ + Jets is completely irreducible. These are generally di-jet topologies. At higher jet multiplicities top quark production followed by semi-leptonic top decay accounts of the largest background. These backgrounds are predicted using a well understood control sample this is fully explained in Section 7.6.

The final background source is that introduced by detector failure or electronic noise induced by the movement of the L.H.C proton beam. Approximately 1% of the ECAL read out is not available in offline event reconstruction, this provides a source of fake missing energy.

7.2 The α_T variable.

α_T is inspired by Ref [10] and was expanded to transverse multi jet topologies by members of the CMS collaboration in Refs [5, 6]. The purpose is to provide a variable that can be cut on to eliminate QCD from the final selection. To do this the inherent balance of the QCD system is exploited.

For di-jet systems α_T is defined as:

$$\alpha_T = \frac{E_{\mathrm{T}}^{j_2}}{M_T} \tag{7.1}$$

where $E_{\mathrm{T}}{}^{j_2}$ is the transverse energy of least energetic of the two jets and M_T is defined as:

$$M_T = \sqrt{\left(\sum_{i=1}^{2} E_{\mathrm{T}}^{j_i}\right)^2 - \left(\sum_{i=1}^{2} p_x^{j_i}\right)^2 - \left(\sum_{i=1}^{2} p_y^{j_i}\right)^2} \tag{7.2}$$

For a perfectly measured di-jet system with $E_{\mathrm{T}}{}^{j_1} = E_{\mathrm{T}}{}^{j_2}$, where the jets are opposite in ϕ $\alpha_T = 0.5$, for events with back to back jets where one is miss-measured $\alpha_T < 0.5$. However the majority of signals predict many jets in the final state. α_T can be generalised to work with n-jets in the flowing way. The variables H_{T}, $\not{H}_{\mathrm{T}}$ and ΔH_{T} are constructed:

$$H_{\mathrm{T}} = \sum_{i=0}^{n\ jets} E_{\mathrm{T}}^{jet_i} \tag{7.3}$$

$$\not{H}_{\mathrm{T}} = \left| \sum_{i=0}^{n\ jets} \vec{p}_T^{\,jet_i} \right| \tag{7.4}$$

for jets above some predefined threshold E_{T} which is common for all jet based quantities. The multi jet system is reduced to a pseudo di-jet system by forming two large jets. The individual jet E_{T}'s are summed, with the final configuration being chosen to have the minimum difference in energy (ΔH_{T}) between the pseudo jets. This simple clustering criteria provides the best separation between miss-measured events and those with real $\not{E}_{\mathrm{T}}$.

α_T is then defined as:

$$\alpha_T = \frac{H_{\mathrm{T}} - \Delta H_{\mathrm{T}}}{2\sqrt{H_{\mathrm{T}}^2 - \not{H}_{\mathrm{T}}^2}} \tag{7.5}$$

Figure 7.1 shows the α_T distribution for both data and simulated background samples. The QCD multi jet background is negligible above an α_T value of 0.55, where as the standard model processes which involve real $\not{E}_{\mathrm{T}}$ exist at all possible values of α_T. Values of α_T in the range $0.5 < \alpha_T < 0.55$ arise in multi jet QCD due to jets falling below threshold or large stochastic fluctuations. It is to be noted that the discrepancy between data and simulation for $\alpha_T \leq 0.55$ is due to no trigger emulation being applied to the simulated background samples.

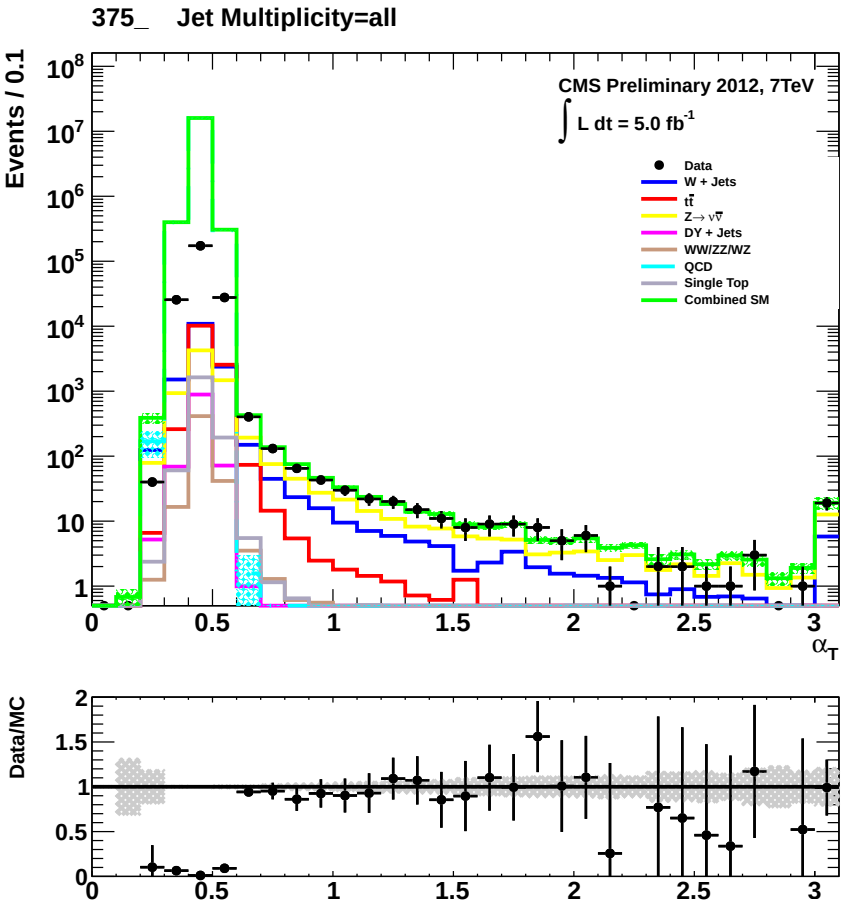

Figure 7.1: α_T distribution for background and data. Trigger emulation is not applied in the simulated background which leads to the discrepancy in the region $\alpha_T \leq 0.55$. The QCD multi-jet background is reduced to less than one event.

7.3 Event selection

7.4 High Level triggers for the α_T analysis

The CMS trigger system has been discussed in detail in Section 3.1 and Chapter 5, however details of analysis specific trigger paths were not discussed. During 2011 the first α_T specific trigger was designed and deployed online. The trigger was then upgraded for the higher luminosity and energy conditions of the 2012 data taking period.

The trigger takes advantage of cutting on two variables, H_{T} and α_T at low H_{T} a high α_T value cuts the trigger rate, where as at high H_{T} where the trigger rate is lower the α_T requirement can be loosened.

Due to the scaling of jet thresholds in the lowest offline H_{T} bins as detailed in Section 7.3 using a fixed jet threshold would cause inefficiency in the lowest offline H_{T} bins. To over come this the trigger level α_T calculation is performed iteratively for all jets above a predefined threshold. This raises the total number of accepted events whilst adding the benefit of being efficient for any offline jet threshold above the minimum trigger jet threshold. The algorithm is show in Figure 7.2.

7.5 2011 Trigger

Due to concerns on the time taken to perform the ΔH_{T} minimisation at the trigger and time constraints enforced on trigger menu development, the first implementation calculates α_T for the first 3 jets. For higher jet multiplicities the variable β_T is calculated.

$$\beta_T = \frac{H_{\mathrm{T}}}{2\sqrt{H_{\mathrm{T}}^2 - \not{H}_{\mathrm{T}}^2}} \tag{7.6}$$

this gives us the relation:

$$\alpha_T \leq \beta_T. \tag{7.7}$$

The decision flow is shown in Figure 7.2 and explained in detail below.

When a level one accept is issued the trigger bits that fired are checked, if the event fires a L1 muon trigger it is passed to the HLT muon triggers where only muon reconstruction is performed, reducing the reconstruction time. The α_T triggers are seeded on the lowest threshold unprescaled L1 H_{T} trigger, during 2011 this was L1_HTT100. Any events issuing a L1 accept and passing L1_HTT100 undergo calorimeter jet reconstruction, the reconstruction algorithm is detailed in Section 4.1.

Once the jets have been formed the trigger filter is entered. Initially the first two jets ranked by E_{T}, are considered, H_{T} and α_T are calculated, if both pass the trigger thresholds the event is accepted and the full detector read out is performed. If either H_{T} or α_T is below threshold, the next jet in E_{T} order is added, if the jet collection contains more than 3 jets then the β_T approximation is used. All jets in the event are added until either the even is accepted, or there are no more jets to be added above 40 GeV.

The effect of switching to the β_T approximation is to accept events that have missing energy due to miss-measurement, when calculating α_T offline these events have values of $\alpha_T < 0.5$. This introduces an impurity to the trigger and costs rate for events that will not be considered in the offline analysis.

7.5.1 Trigger efficiency measurement

The performance of the α_T trigger suit is measured with respect to a sample collected using the muon system. This allows the measurement of efficiency of both the level one seed trigger and the higher level trigger at the same time as different sub-systems are used to collect the reference and the signal triggers. This is due to the exclusive use of calorimeter jets in the α_T trigger, if more complicated reconstruction methods which produce an event hypothesis were used, muons would at HLT level only be considered as jets. Where as during calorimeter only reconstruction, muons are not considered and the p_{T} of any muons in an event is viewed as missing energy.

7.6 Electro-Weak background prediction

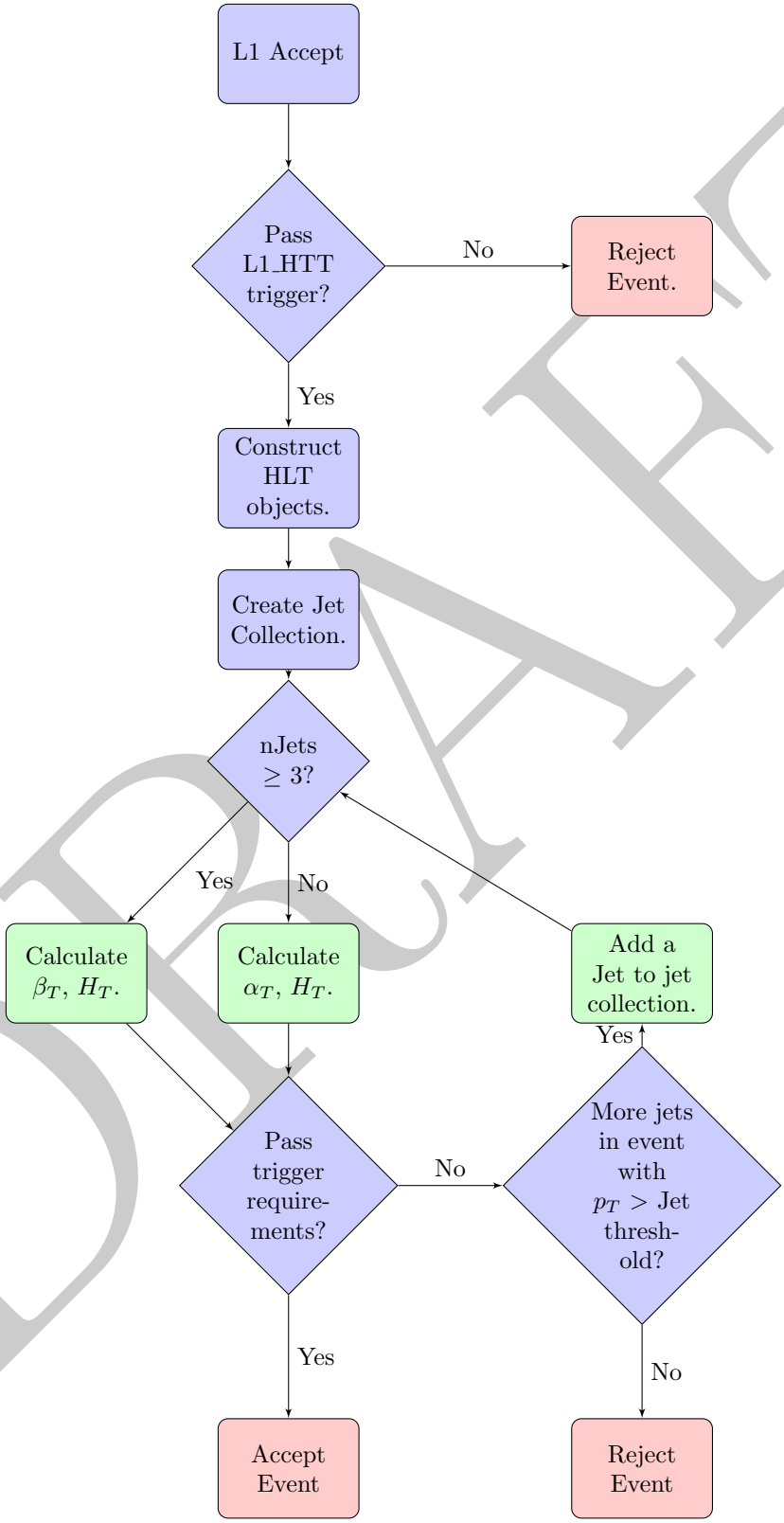

Figure 7.2: Flow chart representing the steps taken to make a trigger decision using the α_T trigger algorithm.

Chapter 8

Conclusion

1

Bibliography

[1] T Åkesson. The ATLAS experiment at the CERN Large Hadron Collider - CERN Document Server. *Particles*, 1999.

[2] B Alessandro, F Antinori, J Belikov, and C Blume. ALICE: Physics performance report, volume II. *Journal of Physics G: Nuclear and Particle Phyiscs*, January 2006.

[3] Michael Benedikt, Paul Collier, V Mertens, John Poole, and Karlheinz Schindl. *LHC Design Report*. CERN, Geneva, 2004.

[4] CMS Collaboration. The Trigger and Data Acquisition Project Technical Design Report, Volume 1, The Level-1 Trigger. *CERN/LHCC 2000-038, CMS TDR 6.1*, 2000.

[5] CMS Collaboration. SUSY searches with dijet events. Technical report, 2008.

[6] CMS Collaboration. Search strategy for exclusive multi-jet events from supersymmetry at CMS. Technical report, 2009.

[7] M Friedl, N Frischauf, T Bauer, T Bergauer, W Waltenberger, A R Knapitsch, C Irmler, I Kratschmer, W Treberer-treberspurg, B Rahbaran, V Innocente, T Camporesi, S Gowdy, L Malgeri, A Marchioro, L Moneta, W Weingarten, M Giunta, M Rovere, A Bonato, A C Spataru, S Zhang, A Perieanu, N Heracleous, H K V Reithler, B Philipps, M K Merschmeyer, C A Heidemann, H Geenen, Y Kuessel, E Kuznetsova, J Olzem, A Bethani, L Calligaris, R Walsh bastos rangel, T M M Dorland, G Quast, A H Dierlamm, I Katkov, R M Ulrich, F M H Stober, C Barth, X Mol, A Kornmayer, F Matorras, A Calderon tazon, A Lopez garcia, J A Brochero cifuentes, M J Bercher, M Haguenauer, Y Sirois, C M Mironov, P Depasse, L Sgandurra, G P Heath, Z Meng, D A Hartley, N I Geddes, S Quinton, I R Tomalin, K Harder, V B Francis, Z Zhang, T Geralis, D Loukas, I Topsis giotis, G Bencze, S T Hernath, I Szeberenyi, S Banerjee, S Singh, A Colaleo, G P Maggi, M Maggi, F Loddo,

R Campanini, I D'antone, C Grandi, L Guiducci, M Gulmini, S Fantinel, P Meridiani, K K Joo, S Song, J Rhee, E Won, M Jo, H Kim, D H Kim, G N Kim, J E Kim, T Son, W M Dominik, K Bunkowski, J C Rasteiro da silva, J Varela, A Alves, V Sulimov, A Vorobyev, V Murzin, S Lukyanenko, G Mesyats, V Postoev, A Pashenkov, A Solovey, S Troitsky, N Lychkovskaya, G Safronov, A Fedotov, K Olimov, M Fazilov, A Umaraliev, I Dumanoglu, N M Bakirci, C Dozen, M Zeyrek, M Yalvac, S Ozkorucuklu, K Sevim, Y Chang, W T Lin, S Bahinipati, K A Biery, E E Gottschalk, K Maeshima, T Kramer, S W L Kwan, S J Murray, L Taylor, N Mokhov, J M Marraffino, S Mrenna, V Yarba, B Banerjee, V D Elvira, D C Hare, B Holzman, F X Yumiceva del pozo, W Dagenhart, C L Dumitrescu, S C Ryu, B J Kilminster, J K Adelman-mc carthy, V E Bazterra, I Bucinskaite, P E Karchin, J R Incandela, M D'Alfonso, R Rossin, C A West, J L Gran, G Zilizi, P P Raics, A Bhardwaj, M Naimuddin, A Kumar, N Smiljkovic, C P De oliveira martins, M Petek, A Vercosa custodio, E J Tonelli manganote, M T Narjanen, P Graehling, F Blekman, J M Keaveney, S Blyweert, N van Remortel, X J Janssen, D Druzhkin, M Bansal, A Aleksandrov, M F Shopova, T R Fernandez perez tomei, C Krug, A A Shinoda, T V Rohe, P Arce, M Daniel, J J Navarrete marin, I Redondo fernandez, A Guirao elias, J Santaolalla camino, J Lottin, P Gras, F Kircher, B Levesy, A Payn, A K Nayak, V Bhatnagar, C Randieri, M Bruzzi, O Starodubtsev, A Tropiano, D Piccolo, C Sciacca, S Meola, A Saccomanno, M Esposito, P Azzi, E Conti, S Lacaprara, M Margoni, M Sgaravatto, N Pozzobon, P Torre, B Checcucci, L Fanò, S Taroni, A Lucaroni, F Romeo, G Bagliesi, M A Ciocci, A Giassi, T Boccali, S Arezzini, A Rizzi, G Broccolo, D Dattola, C Mariotti, A Ballestrero, E Camacho-Pérez, R Magaña-Villalba, J Martínez-Ortega, M Górski, G Wrochna, M J Bluj, A Zarubin, M Nozdrin, V Ladygin, A Golunov, A Sotnikov, N Evdokimov, I Lokhtin, A Ershov, N Tyurin, S Akimenko, V Talov, N Belikov, A Ryazanov, G W Hou, Y Chao, J Alwall, X Shi, D R Wood, D C Baumgartel, J Zhang, P D Luckey, K C Sumorok, G Gomez ceballos retuerto, S H Jaditz, G S Stephans, T Ma, P J Lehtonen, M H Chan, I J Moult, R A Ofierzynski, A Pozdnyakov, B L Pollack, P B Padley, A H Adair, W J Clarida, E Tiras, G Cerizza, M Pieri, V A Sharma, M W Lebourgeois, M Norman, F Golf, M J Murray, J L S Bowen, K Buterbaugh, M Sharma, J Bunn, H Newman, M Gataullin, M Spiropulu, J Veverka, S D Thomas, K J Rose, S M Panwalkar, A Calamba, Z Xie, J S Werner, A M Zuranski, A Ferapontov, E M Laird, G Kukartsev, Z Mao, S J Wimpenny, S Gleyzer, M G Weinberg, V Veeraraghavan, and J... Bochenek. CMS - The Compact Muon Solenoid. January 1996.

[8] J Marrouche and others. Commissioning the CMS Global Calorimeter Trigger. *CMS*

IN, 2010/029, 2010.

[9] J Rademacker. LHCb: Status and Physics Prospects. *Arxiv preprint hep-ex*, January 2005.

[10] Lisa Randall and David Tucker-Smith. Dijet Searches for Supersymmetry at the LHC. *arXiv*, hep-ph, January 2008.

[11] C Wulz. The CMS experiment at CERN. *cdsweb.cern.ch*.